Acta Crystallographica Section F
Structural Biology and Crystallization Communications
ISSN 1744-3091

Preliminary joint X-ray and neutron protein crystallographic studies of endoxylanase II from the fungus *Trichoderma longibrachiatum*

Andrey Y. Kovalevsky,[a]* B. Leif Hanson,[b] Sean Seaver,[b] S. Zoë Fisher,[a] Marat Mustyakimov[a] and Paul Langan[a]

[a]Bioscience Division, MS M888, Los Alamos National Laboratory, Los Alamos, NM 87545, USA, and [b]Department of Chemistry, University of Toledo, Toledo, OH 53606, USA

Correspondence e-mail: ayk@lanl.gov

Received 21 September 2010
Accepted 14 December 2010

Room-temperature X-ray and neutron diffraction data were measured from a family 11 endoxylanase holoenzyme (XynII) originating from the filamentous fungus *Trichoderma longibrachiatum* to 1.55 Å resolution using a home source and to 1.80 Å resolution using the Protein Crystallography Station at LANSCE. Crystals of XynII, which is an important enzyme for biofuel production, were grown at pH 8.5 in order to examine the effect of basic conditions on the protonation-state distribution in the active site and throughout the protein molecule and to provide insights for rational engineering of catalytically improved XynII for industrial applications.

1. Introduction

Lignocellulosic biomass, a fibrous material derived from plant cell walls comprised of lignin, hemicellulose and cellulose, is a potential clean and renewable nonfood carbon-based feedstock for fuel and chemical production, in much the same way as crude oil serves as the carbon feedstock in petrochemical refineries (Carroll & Somerville, 2009). In particular, the sugars derived from the cellulosic and hemicellulosic portions of biomass can be converted to biofuels or other value-added products using current technologies. The deconstruction of biomass into simple sugars constitutes a core barrier for producing products from the sugar platform. Recently, a combination of novel mild pretreatment techniques and enzymatic hydrolysis with cocktails of cellulolytic enzymes has led to improved yields of monosaccharides relative to thermochemical methods, while also lowering the amounts of fermentation inhibitors (Berlin *et al.*, 2006; Lau *et al.*, 2008; da Costa Sousa *et al.*, 2009; Lau & Dale, 2009). Furthermore, the supplementation of these cellulase mixtures with hemicellulases (*i.e.* endo-β-1,4-xylanases and β-xylosidases) has demonstrated synergistic effects during saccharification, increasing the yield of pentose sugars in biomass hydrolysates (Gupta *et al.*, 2008; Zhong *et al.*, 2009; Gao *et al.*, 2010).

Xylanases (endo-β-1,4-xylanases; EC 3.2.1.8) are glycoside hydrolases that cleave the internal (endo) β-1,4-xylosidic linkages of xylan, causing the depolymerization of this most abundant hemicellulose and generating smaller oligosaccharide chains. Bacterial and fungal xylanases are mesophilic enzymes, with optimal performance at slightly elevated temperatures (~323–328 K) and in acidic conditions at pH ~5–6 (Collins *et al.*, 2005; Polizeli *et al.*, 2005). We are investigating several xylanases with a view to understanding their detailed catalytic and substrate-binding mechanisms and the dependence of these mechanisms on pH and temperature. This new information is then being exploited to re-engineer the xylanases so that their biocatalyses are more effective at lower temperatures and higher pH values, thus improving the energy efficiency and lowering the cost of biomass saccharification.

Like other retaining endoxylanases, the family 11 xylanase (XynII) from the filamentous fungus *Trichoderma longibrachiatum* (formerly *T. reesei*; Wong *et al.*, 1988) hydrolyzes the ether-like links between the main-chain xylose units in xylan with retention of the anomeric

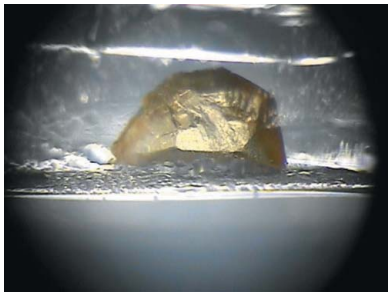

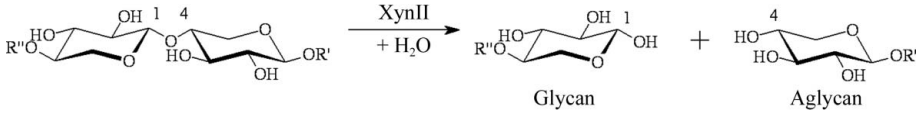

Figure 1
Depolymerization reaction of xylan catalyzed by XynII. The second step of the hydrolysis requires an incoming catalytic water molecule activated by the enzyme. XynII cleaves 1,4-β-ether linkages between the xylose subunits (connected by C atoms C1 and C4).

C-atom (C1) stereochemistry (Fig. 1). Two distinct catalytic mechanisms have been proposed for the enzyme. Both involve two catalytic Glu residues, Glu86 and Glu177, with the latter being protonated and acting as a general acid. In the double-displacement pathway, a putative covalent intermediate with an inverted C1 center is formed in the active site, directly connecting C1 of the reducing (glycan) end of the xylan chain and a carboxylic group of one of the two catalytic Glu residues (Rye & Withers, 2000). In an alternative proposal, a carbocation with the positive charge localized on the C1 atom is generated and is stabilized by the negative charges on the Glu residues (Törrönen & Rouvinen, 1997). The resulting covalent enzyme–substrate complex or the carbocation is hydrolyzed off or hydrated, respectively, by an incoming water molecule, which is activated by the second Glu, to give the glycan product with overall retention of stereochemistry. Several X-ray structural studies of family 11 xylanases from *Bacillus* species offer support for the double-displacement pathway (Havukainen *et al.*, 1996; Sabini *et al.*, 1999, 2001; Sidhu *et al.*, 1999). However, these proposed biochemical reactions involve the transfer of hydrogen, which is difficult to locate using X-ray crystallography. Consequently, neither proposal has been unambiguously verified. It has not even been possible to verify the protonation of the key catalytic residue, Glu177, in both proposals.

Hydrogen (and its isotope deuterium) can be more easily located using neutrons (Niimura & Bau, 2008; Blakeley, Langan *et al.*, 2008), and we are using the Protein Crystallography Station (PCS) built at the spallation neutron source run by Los Alamos Neutron Scattering Center (LANSCE) at Los Alamos National Laboratory (Langan *et al.*, 2004) to reveal the location and movement of hydrogen in this enzymatic process. Furthermore, we are combining neutron data collected on the PCS with X-ray data in a joint X-ray/neutron (XN) analysis so that more accurate and complete structures can be obtained (Adams *et al.*, 2009). This joint XN approach has recently been used to reveal new information on the catalytic mechanisms of several other enzymes (Adachi *et al.*, 2009; Blakeley, Ruiz *et al.*, 2008; Blum *et al.*, 2009; Coates *et al.*, 2008; Fisher *et al.*, 2007, 2010; Kovalevsky, Hanson *et al.*, 2010; Kovalevsky, Fisher *et al.*, 2010; Oksanen *et al.*, 2009; Yamaguchi *et al.*, 2009). Here, we report the optimization of crystallization conditions for XynII at pH 8.5, which has allowed the collection of room-temperature neutron and X-ray data from crystals harvested from the same drop. This represents the first study of a xylanase, or indeed any type of glycosidase, using neutron crystallographic data.

2. Crystallization

XynII was purchased from Hampton Research (Aliso Viejo, California, USA) as a 36 mg ml^{-1} slurry in 43% glycerol. For crystallization trials, the commercial sample was further purified on a desalting column (HiPrep 26/10; GE Healthcare, Piscataway, New Jersey, USA) with 0.1 *M* Tris buffer pH 8.5. Although successful, crystallization attempts using the previously published PEG 8000/calcium chloride (Moiseeva & Allaire, 2004) or ammonium sulfate/sodium iodide (Watanabe *et al.*, 2006) conditions did not result in crystals of sufficient size or quality for room-temperature X-ray or neutron crystallography. By altering the conditions, large yellow crystals were obtained by the sitting-drop vapor-diffusion method with a reservoir solution consisting of 10% PEG 8000, 0.2 *M* sodium iodide and 0.1 *M* Tris pH 8.5. The starting enzyme concentration was 21–23 mg ml^{-1}. Crystallization growth was scaled up by using nine-well siliconized glass plates and the sandwich-box setup (Hampton Research). The large setup involved 800 µl crystallization drops (400 µl enzyme + 400 µl mother liquor) and 50 ml reservoir solution and produced XynII crystals as large as 6–7 mm^3 in volume, which is more than sufficient for neutron crystallography.

3. Data collection and reduction

3.1. Neutron crystallography

Several of the largest crystals were successfully mounted in quartz capillaries (Fig. 2) with an inner diameter of 4 mm. The capillaries were reshaped as an hourglass to prevent crystal slippage and solvent reaching the crystal. Deuterated buffer (∼0.5 ml) was placed in the lower part of the capillary. H/D vapor exchange was allowed to occur in the capillary for several months before the collection of neutron diffraction data. A 24 h test exposure was taken from the first crystal, yielding neutron diffraction to ∼2.0 Å resolution. The diffraction quality and the signal-to-noise ratio were deemed to be suitable for collection of a full data set (Fig. 3).

Time-of-flight wavelength-resolved Laue images were collected at room temperature on a Huber κ-circle goniometer at 35 usable settings. The first seven of these settings were collected during the 2009 LANSCE run cycle with an exposure time of 24 h per setting and yielded diffraction data to about 2.0 Å resolution. However, after the installation of a new tungsten spallation neutron target and moderator system (MACH-III) at the Lujan Center at LANSCE at the beginning of 2010, the neutron flux on the PCS has improved several-fold. We were therefore able to reduce the exposure time per frame to 10–16 h for the remaining 28 settings and also to collect

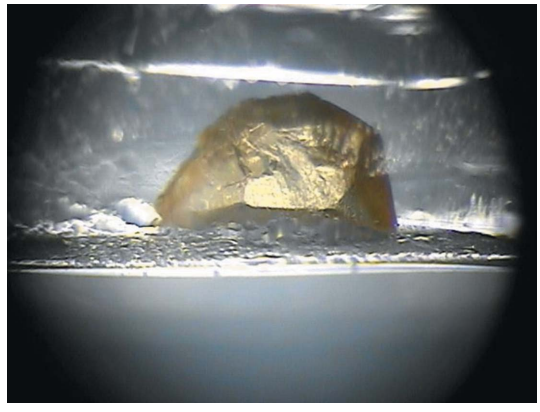

Figure 2
Crystal of XynII used for neutron diffraction data collection. The crystal was about 3 × 2 × 1.2 mm in size (∼7 mm^3) and was mounted in an hourglass-shaped quartz capillary.

higher resolution data to about 1.80 Å. Because of their improved resolution, only the last 28 settings were used for data processing.

At the PCS, the crystal-to-detector distance is set to 730 mm, corresponding to the cylindrical radius of the detector, while the detector is normally kept at $2\theta = 0^\circ$ during the entire experiment, effectively collecting data in the $\pm 60^\circ$ 2θ range and $\pm 8^\circ$ in the vertical direction. The full data set was collected by reorienting the crystal using the κ and ω goniometer circles and measuring diffraction frames while performing φ step-scans of 30° at each crystal orientation. Each image was processed using a version of *d*TREK* (Pflugrath, 1999) modified for wavelength-resolved Laue neutron protein crystallography (Langan & Greene, 2004). The integrated reflections were wavelength-normalized using *LAUENORM* (Helliwell *et al.*, 1989) and then merged using *SCALA* as incorporated into *CCP*4 (Evans, 2006; Diederichs & Karplus, 1997; Weiss & Hilgenfeld, 1997; Collaborative Computational Project, Number 4, 1994). The 'tails' of the wavelength range were cut off, with a restricted range of 0.73–3.50 Å, from the original 0.6–7.0 Å wavelength distribution of the thermal neutrons in order to remove the least accurately measured reflections. The overall completeness was 88.0% to 1.80 Å, with an $R_{\rm merge}$ of 23.0% and a redundancy of 3.5 for the orthorhombic space group $P2_12_12_1$. The crystallographic statistics are presented in Table 1.

3.2. X-ray crystallography

An X-ray crystallographic data set was collected to 1.55 Å resolution at 293 K in-house from a crystal of XynII sealed in a thin-walled quartz capillary with D_2O buffer using a Rigaku FR-E diffractometer equipped with an R-AXIS VI^{++} detector. Diffraction data were integrated and scaled using the *CrystalClear*/*d*TREK* software (Pflugrath, 1999) and structure refinement is in progress using *SHELX* (Sheldrick, 2008). A room-temperature X-ray data set obtained from an isomorphous crystal is essential for the success of joint XN structure refinement. We ensured this by taking the crystal for the X-ray data collection from the same crystallization drop and sealing it in a capillary with identical D_2O buffer. A summary of the crystallographic data is given in Table 1.

3.3. Preliminary XN analysis

Joint X-ray and neutron (XN) refinement of the structure is in progress utilizing the program *nCNS* (Adams *et al.*, 2009), which was modified from *CNS* (Brünger *et al.*, 1998) and allows the use of both neutron and X-ray data in structural refinement. Initial nuclear scattering density maps calculated after rigid-body refinement show the clear features usually observed in nuclear scattering density maps. D atoms on the hydroxyl and amine/amide groups are visible as strong nuclear density peaks in the $2F_o - F_c$ map, while H atoms at aliphatic and aromatic CH groups are detected as troughs in the $-(2F_o - F_c)$ nuclear scattering density map. Determination and a detailed analysis of the protonation states of the active-site residues and the hydration of XynII will be reported elsewhere.

Table 1
Room-temperature neutron and X-ray diffraction data-collection statistics.

Values in parentheses are for the highest resolution shell.

Source	PCS, LANSCE, LANL	Rigaku FR-E (home source)
Settings	28	180 (1° oscillations)
Space group	$P2_12_12_1$	
Unit-cell parameters (Å)	$a = 49.61$, $b = 60.03$, $c = 70.55$	
Unit-cell volume (Å^3)	210104	
Resolution	23–1.80 (1.90–1.80)	34–1.55 (1.61–1.55)
No. of reflections (measured/unique)	60543/17469	126040/30268
Multiplicity	3.5 (2.2)	4.2 (4.0)
Completeness (%)	88.0 (75.7)	96.8 (93.2)
$R_{\rm merge}$†	0.230 (0.379)	0.069 (0.449)
$R_{\rm p.i.m.}$‡	0.136 (0.280)	n/a
Wavelength range (Å)	0.73–3.5	Monochromatic, 1.5418
$\langle I/\sigma(I)\rangle$	6.5 (3.6)	9.8 (1.9)

† $R_{\rm merge} = \sum_{hkl}\sum_i |I_i(hkl) - \langle I(hkl)\rangle| / \sum_{hkl}\sum_i I_i(hkl)$. ‡ $R_{\rm p.i.m.} = \sum_{hkl}[1/(N-1)]^{1/2} \times \sum_i |I_i(hkl) - \langle I(hkl)\rangle| / \sum_{hkl}\sum_i I_i(hkl)$ (Weiss, 2001).

4. Discussion

This represents the first crystallographic study using neutrons of an endoxylanase, or indeed of any glycosidic enzyme in general, and is therefore likely to provide important new information. The X-ray diffraction data set is one of the highest resolution (1.55 Å) reported so far at room temperature for a family 11 xylanase. To our surprise, the published crystallization conditions that had previously resulted in the highest resolution (1.19 Å) room-temperature XynII structure (Watanabe *et al.*, 2006) failed to produce crystals of sufficient size and quality for room-temperature X-ray and neutron data collection. Only when a combination of PEG 8000 and NaI was used were we able to grow crystals of sufficient size and quality for both room-temperature X-ray and neutron diffraction experiments. In addition, we have discovered that the best crystals grew when the commercial sample was run through a desalting column, effectively removing glycerol from the enzyme solution, even though the user guide supplied by Hampton Research specifically recommends avoiding enzyme dialysis before crystallization. Therefore, it must be emphasized that crystal growth for neutron crystallographic experiments often demands re-evaluation and re-optimization of the published successful crystallization conditions. Crystals of XynII were grown at pH 8.5 in order to determine the effect of basic conditions on the protonation states of the active-site residues and amino-acid side chains throughout the protein. Our hope is that this study, together

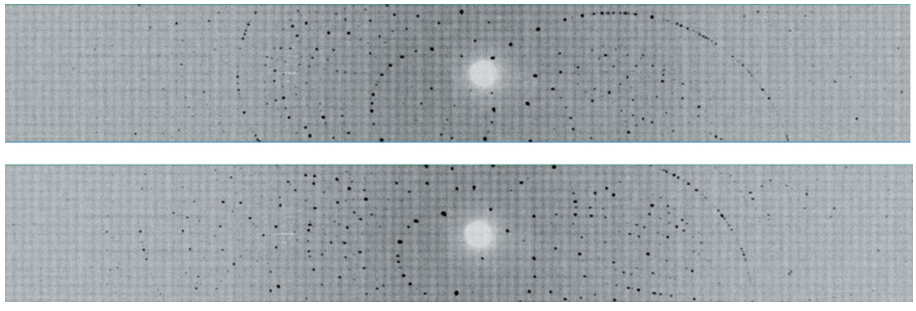

Figure 3
Neutron Laue diffraction pattern for the XynII crystal in two different crystal settings. In each crystal setting the three-dimensional diffraction data were projected in time-of-flight to produce a conventional two-dimensional Laue pattern.

with similar studies that are under way at pH ∼6 and with enzyme–oligosaccharide complexes, will provide a detailed understanding of why activity and substrate affinity drop sharply at high pH values for XynII. These insights will be used to guide rational engineering of the enzyme for improved performance in alkaline solutions.

The PCS is funded by the Office of Biological and Environmental Research of the Department of Energy. MM and PL were partly supported by an NIH–NIGMS-funded consortium (1R01GM071939-01) between LANL and LBNL to develop computational tools for neutron protein crystallography. AYK was partly supported by LANL LDRD grant 20080789PRD3. AYK and PL were partly supported by LANL LDRD grant 20080001DR.

References

Adachi, M., Ohhara, T., Kurihara, K., Tamada, T., Honjo, E., Okazaki, N., Arai, S., Shoyama, Y., Kimura, K., Hayashi, Y., Kiso, Y. & Kuroki, R. (2009). *Proc. Natl Acad. Sci. USA*, **106**, 4641–4646.

Adams, P. D., Mustyakimov, M., Afonine, P. V. & Langan, P. (2009). *Acta Cryst.* D**65**, 567–573.

Berlin, A., Balakshin, M., Gilkes, N., Kadla, J., Maximenko, V., Kubo, S. & Saddler, J. (2006). *J. Biotechnol.* **125**, 198–209.

Blakeley, M. P., Langan, P., Niimura, N. & Podjarny, A. (2008). *Curr. Opin. Struct. Biol.* **18**, 593–600.

Blakeley, M. P., Ruiz, F., Cachau, R., Hazemann, I., Meilleur, F., Mitschler, A., Ginell, S., Afonine, P., Ventura, O. N., Cousido-Siah, A., Haertlein, M., Joachimiak, A., Myles, D. & Podjarny, A. (2008). *Proc. Natl Acad. Sci. USA*, **105**, 1844–1848.

Blum, M. M., Mustyakimov, M., Rüterjans, H., Schoenborn, B. P., Langan, P. & Chen, J. C.-H. (2009). *Proc. Natl Acad. Sci. USA*, **106**, 713–718.

Brünger, A. T., Adams, P. D., Clore, G. M., DeLano, W. L., Gros, P., Grosse-Kunstleve, R. W., Jiang, J.-S., Kuszewski, J., Nilges, M., Pannu, N. S., Read, R. J., Rice, L. M., Simonson, T. & Warren, G. L. (1998). *Acta Cryst.* D**54**, 905–921.

Carroll, A. & Somerville, C. (2009). *Annu. Rev. Plant Biol.* **60**, 165–182.

Coates, L., Tuan, H. F., Tomanicek, S., Kovalevsky, A. Y., Mustyakimov, M., Erskine, P. & Cooper, J. (2008). *J. Am. Chem. Soc.* **130**, 7235–7237.

Collaborative Computational Project, Number 4 (1994). *Acta Cryst.* D**50**, 760–763.

Collins, T., Gerday, C. & Feller, G. (2005). *FEMS Microbiol. Rev.* **29**, 3–23.

Diederichs, K. & Karplus, P. A. (1997). *Nature Struct. Biol.* **4**, 269–275.

Da Costa Sousa, L., Chundawat, S. P., Balan, V. & Dale, B. E. (2009). *Curr. Opin. Biotechnol.* **20**, 339–347.

Evans, P. (2006). *Acta Cryst.* D**62**, 72–82.

Fisher, S. Z., Anderson, S., Henning, R., Moffat, K., Langan, P., Thiyagarajan, P. & Schultz, A. J. (2007). *Acta Cryst.* D**63**, 1178–1184.

Fisher, S. Z., Kovalevsky, A., Mustyakimov, M., McKenna, R., Silverman, D. & Langan, P. (2010). *Biochemistry*, **49**, 415–421.

Gao, D., Chundawat, S. P. S., Krishnan, C., Balan, V. & Dale, B. E. (2010). *Bioresour. Technol.* **101**, 2770–2781.

Gupta, R., Kim, T. H. & Lee, Y. Y. (2008). *Appl. Biochem. Biotechnol.* **148**, 59–70.

Havukainen, R., Törrönen, A., Laitinen, T. & Rouvinen, J. (1996). *Biochemistry*, **35**, 9617–9624.

Helliwell, J. R., Habash, J., Cruickshank, D. W. J., Harding, M. M., Greenhough, T. J., Campbell, J. W., Clifton, I. J., Elder, M., Machin, P. A., Papiz, M. Z. & Zurek, S. (1989). *J. Appl. Cryst.* **22**, 483–497.

Kovalevsky, A. Y., Fisher, S. Z., Seaver, S., Mustyakimov, M., Sukumar, N., Langan, P., Mueser, T. C. & Hanson, B. L. (2010). *Acta Cryst.* F**66**, 474–477.

Kovalevsky, A. Y., Hanson, B. L., Fisher, S. Z., Mason, S. A., Forsyth, V. T., Blakeley, M. P., Keen, D. A., Wagner, T., Carrell, H. L., Katz, A. K., Glusker, J. P. & Langan, P. (2010). *Structure*, **18**, 688–699.

Langan, P. & Greene, G. (2004). *J. Appl. Cryst.* **37**, 253–257.

Langan, P., Greene, G. & Schoenborn, B. P. (2004). *J. Appl. Cryst.* **37**, 24–31.

Lau, M. W. & Dale, B. E. (2009). *Proc. Natl Acad. Sci. USA*, **106**, 1368–1373.

Lau, M. W., Dale, B. E. & Balan, V. (2008). *Biotechnol. Bioeng.* **99**, 529–539.

Moiseeva, N. & Allaire, M. (2004). *Acta Cryst.* D**60**, 1275–1277.

Niimura, N. & Bau, R. (2008). *Acta Cryst.* A**64**, 12–22.

Oksanen, E., Blakeley, M. P., Bonneté, F., Dauvergne, M. T., Dauvergne, F. & Budayova-Spano, M. (2009). *J. R. Soc. Interface*, **6**, S599–S610.

Pflugrath, J. W. (1999). *Acta Cryst.* D**55**, 1718–1725.

Polizeli, M. L. T. M., Rizzatti, A. C. S., Monti, R., Terenzi, H. F., Jorge, J. A. & Amorim, D. S. (2005). *Appl. Microbiol. Biotechnol.* **67**, 577–591.

Rye, C. S. & Withers, S. G. (2000). *Curr. Opin. Chem. Biol.* **4**, 573–580.

Sabini, E., Sulzenbacher, G., Dauter, M., Dauter, Z., Jørgensen, P. L., Schülein, M., Dupont, C., Davies, G. J. & Wilson, K. S. (1999). *Chem. Biol.* **6**, 483–492.

Sabini, E., Wilson, K. S., Danielsen, S., Schülein, M. & Davies, G. J. (2001). *Acta Cryst.* D**57**, 1344–1347.

Sheldrick, G. M. (2008). *Acta Cryst.* A**64**, 112–122.

Sidhu, G., Withers, S. G., Nguyen, N. T., McIntosh, L. P., Ziser, L. & Brayer, G. D. (1999). *Biochemistry*, **38**, 5346–5354.

Törrönen, A. & Rouvinen, J. (1997). *J. Biotechnol.* **57**, 137–149.

Watanabe, N., Akiba, T., Kanai, R. & Harata, K. (2006). *Acta Cryst.* D**62**, 784–792.

Weiss, M. S. (2001). *J. Appl. Cryst.* **34**, 130–135.

Weiss, M. S. & Hilgenfeld, R. (1997). *J. Appl. Cryst.* **30**, 203–205.

Wong, K. K. Y., Tan, L. U. L. & Saddler, J. N. (1988). *Microbiol. Rev.* **52**, 305–317.

Yamaguchi, S., Kamikubo, H., Kurihara, K., Kuroki, R., Niimura, N., Shimizu, N., Yamazaki, Y. & Kataoka, M. (2009). *Proc. Natl Acad. Sci. USA*, **106**, 440–444.

Zhong, C., Lau, M. W., Balan, V., Dale, B. E. & Yuan, Y.-J. (2009). *Appl. Microbiol. Biotechnol.* **84**, 667–676.